Michael B. Sano[1]
Alireza Salmanzadeh[1,2]
Rafael V. Davalos[1,2]

[1]School of Biomedical Engineering and Sciences, Virginia Tech-Wake Forest University, Blacksburg, VA, USA

[2]Department of Engineering Science and Mechanics, Virginia Tech, Blacksburg, VA, USA

Received December 9, 2011
Revised April 8, 2012
Accepted April 9, 2012

Research Article

Multilayer contactless dielectrophoresis: Theoretical considerations

Dielectrophoresis (DEP), the movement of dielectric particles in a nonuniform electric field, is of particular interest due to its ability to manipulate particles based on their unique electrical properties. Contactless DEP (cDEP) is an extension of traditional and insulator-based DEP topologies. The devices consist of a sample channel and fluid electrode channels filled with a highly conductive media. A thin insulating membrane between the sample channel and the fluid electrode channels serves to isolate the sample from direct contact with metal electrodes. Here we investigate, for the first time, the properties of multilayer devices in which the sample and electrode channels occupy distinct layers. Simulations are conducted using commercially available finite element software and a less computationally demanding numerical approximation is presented and validated. We show that devices can be created that achieve a similar level of electrical performance to other cDEP devices presented in the literature while increasing fluid throughput. We conclude, based on these models, that the ultimate limiting factors in device performance resides in breakdown voltage of the barrier material and the ability to generate high-voltage, high-frequency signals. Finally, we demonstrate trapping of MDA-MB-231 breast cancer cells in a prototype device at a flow rate of 1.0 mL/h when 250 V_{RMS} at 600 kHz is applied.

Keywords:
Cancer detection / High throughput / Microfluidics / Numerical model / Rare cell isolation
DOI 10.1002/elps.201100677

1 Introduction

Dielectrophoresis (DEP), the movement of dielectric particles in a nonuniform electric field, is of particular interest due to its ability to manipulate particles based on their size, shape, and unique electrical properties. This phenomenon was first reported by Pohl who described the motion of particles under the influence of a nonuniform electric field in a ring-and-pin electrode geometry [1]. Further experiments conducted with both direct current (DC) and alternating current (AC) signals proved that this particle motion was independent of the previously known electrokinetic phenomenon in which particles move under the influence of a uniform electric field. These experiments were conducted in 10-cm petri dishes, and other macroscale environments, in which inertial forces dominate allowing for chaotic flow instabilities, eddies, and vortices to develop. Despite this, Pohl and others were able to isolate particles in large quantities from a suspending medium [2] and separate living and dead cells [3] using DEP.

Correspondence: Michael B. Sano, School of Biomedical Engineering and Sciences, Virginia Tech-Wake Forest University, 329 ICTAS Building, Stanger Street (MC 0298), Blacksburg, VA 24061, USA
E-mail: sano@vt.edu
Fax: +1-540-231-9738

Abbreviations: cDEP, contactless dielectrophoresis; **C–M**, Clausius–Mossoti; **iDEP**, insulator-based dielectrophoresis

Microfluidic cell sorting, isolation, and enrichment technologies have evolved rapidly over the past two decades, thanks in part to the rapid advances in microfabrication techniques. Using a microfabricated array of parallel electrodes patterned on the bottom of a microfluidic channel, Fuhr et al. demonstrated the ability to induce translational motion of particles and cells using a phase shifted electric field [4]. This technique, known as traveling wave DEP (twDEP) [5], has since been used to enrich latex particles [5, 6] and dormant protozoa [7], and sort populations of living cells [8]. Additionally, electrodes patterned on the bottom of a microfluidic channel can be used to trap cells as they flow through the channel [9]. This technique has been demonstrated using interdigitated, castellated, and pin–plate geometry electrodes to trap DNA [10], viruses [11], and cells [12–14]. Recently, these devices have also been demonstrated as a rapid method for determining antigen expression and blood typing [15].

One limitation of these devices is that the intensity of the DEP force declines as particles move further from the electrodes surface. This has been addressed with the development of three-dimensional (3D) electrodes that extend from channel floor to ceiling. These devices can be produced by carbonizing photoresist [16], electroplating structures with gold [17], or selectively doping polymers [18].

Alternatively, a nonuniform electric field can be generated by applying a voltage across a channel containing

Colour Online: See the article online to view Figs. 1 and 4 in colour.

insulating structures [19]. The electric field cannot penetrate these insulating features and current is forced to flow around them. This deforms the electric field creating a nonuniformity that induces a DEP force. This technique, known as insulator-based DEP (iDEP), typically employs a static [20] or monopolarity low-frequency voltage [21] to drive sample particles through electrokinetic action, eliminating the need for external pumps. The electric field produced in these devices propagates consistently throughout the height of the sample channel [22], allowing particles to be trapped independent of their location in the z direction. These devices, originally produced in glass [23], can be cast in polymers [24], hot embossed [25], or injection mold [25]. These mass fabrication techniques have the potential to reduce per chip production costs.

It has recently been shown that trapping of cells and particles in iDEP can be accurately predicted using computational modeling providing a robust method to examine devices in silico prior to experimentation [26]. In conjunction with computational methods, this technique can be used to predict the DEP mobility, or induced dipole moment, of cells and particles [27]. iDEP has been demonstrated as an effective method to trap single cells [28], concentrate proteins [29] and DNA [30], separate mixtures of particles [31], and interrogate blood types [32].

Contactless DEP (cDEP) is an extension of traditional and insulator-based DEP topologies [33]. The devices consist of multiple parallel channels: one filled with the sample and others filled with a highly conductive media. A thin (20 μm) insulating membrane between these channels serves to isolate the sample from direct contact with the highly conductive media, which acts as a fluid electrode. When an AC voltage is applied across the fluid electrode channels, capacitive coupling between the electrode channels and the sample channel occurs and a nonuniform electric field is produced within the sample channel. This technique can also be accomplished using a printed circuit board isolated from the sample channel using a microscope cover slip [34].

Numerical and experimental evaluation of these devices indicate that for low fluid velocities, less than 2000 μm/s, the magnitude of the gradient of electric field squared, $|\nabla(\vec{E}\cdot\vec{E})|$, in the sample channel must be approximately 1×10^{12} V^2/m^3 to successfully manipulate cells [35, 36]. Contactless DEP has been used to isolate live cells from dead cells [37] and background particles [38], enrich a population of tumor initiating cells [39], and demonstrate a difference in dielectric properties between breast cancer cell lines [40]. The insulating barriers in a cDEP device act as capacitors, absorbing charge, and eventually blocking the flow of current. To overcome this, the applied voltage must switch at a faster rate than this capacitance can be charged. Typically, cDEP devices require the use of frequencies in excess of 100 kHz.

However, we have recently demonstrated the ability to manipulate cells employing applied potentials with frequencies as low as 1 kHz in a single-layer device [41]. This was accomplished by increasing the capacitance associated with the barriers and increasing the resistance of the sample channel. Here we investigate for the first time, with detailed mathematical modeling, the properties of a multilayer device, in which the sample and fluid electrode channels occupy distinct layers, using finite element software.

Additionally, the resistance and capacitance of the fluid electrodes, sample channel, and insulating barriers are calculated numerically and evaluated as a simple low-pass filter. This is used to predict the device performance characteristics and find an order of magnitude approximate for $|\nabla(\vec{E}\cdot\vec{E})|$. These multilayer devices are electrically similar to single layer devices, maintain compatibility with mass fabrication techniques, and provide a potential method to significantly increase throughput compared to single-layer cDEP devices. Finally, we validate the multilayer cDEP concept with a prototype device. Dielectrophoretic trapping of MDA-MB-231 breast cancer cells is demonstrated under a 250 V_{RMS} potential at 600 kHz and a flow rate of 1.0 mL/h, a 100-fold increase in flow rate over the single-layer version of the same design [35].

2 Theory

Under the influence of a nonuniform AC electric field, cells placed in an infinite ionic liquid become polarized and develop a charge distribution across their volume. Spherical cells are then driven toward the regions of maximum or minimum field gradient by a translational dielectrophoretic force ($\vec{F}_{DEP}$) [42]:

$$\vec{F}_{DEP} = 2\pi\varepsilon_m r^3 \mathrm{Re}[K(\omega)]\nabla(\vec{E}\cdot\vec{E})\cdot[\mathrm{N}] \quad (1)$$

where r is the radius of the cell, ε_m is the permittivity of the suspending medium, and Re[K(ω)] is the real part of the Clausius–Mossotti (C–M) factor. The direction of translational displacement is dependent on the sign of the frequency-dependent C–M factor, which is theoretically bound between –0.5 and 1.0 for spherical particles. This ratio is dependent on the complex conductivity of the cell and the suspending medium. We introduce a particle-independent DEP vector, defined as:

$$\vec{\Gamma} = \frac{\vec{F}_{DEP}}{2\pi\varepsilon_m r^3 \mathrm{Re}[K(\omega)]} = \nabla(\vec{E}\cdot\vec{E})\cdot\left[\frac{V^2}{m^3}\right] \quad (2)$$

to facilitate our discussion of the results. $\vec{\Gamma}$ is a direct measure of a cDEP device's ability to generate DEP forces and will be shown to be highly dependent on frequency, device configuration, and barrier material. This value can be calculated after the potential distribution within the device is determined using multiphysics finite element software. An expanded explanation of the C–M factor and DEP theory can be seen in our previous work [43]. This manuscript will focus on the ability of a multilayer cDEP device to generate a nonuniform electric field within a sample channel. The total DEP force acting on cells within this device geometry will additionally be influenced by the frequency-dependent C–M factor. A review of the geometrical and physical parameters

that may affect experimental results can be found in reference [44].

A cDEP device can be represented as the series combination of three resistors and two resistor–capacitor (RC) pairs in parallel. These represent the impedances of the two fluid electrodes, a single sample channel, and two insulating barriers. In this scenario, the capacitances associated with the sample channel and fluid electrodes are considered negligible. The total impedance (Z_{total}) of this network is easily calculated because all of these elements are in series; the current flowing through each individual RC pair must be the same:

$$Z(\omega)_{total} = 2R_{electrode} + 2R_{sample} + 2\frac{X_{barrier}^2 R_{barrier} - iX_{barrier} R_{barrier}^2}{R_{barrier}^2 + X_{barrier}^2}\,[\Omega] \quad (3)$$

where R is the resistance and X is the capacitive reactance ($X = -1/(\omega C)$). For simplicity, we can neglect the small capacitive elements associated with the fluid electrodes and sample channel as their capacitance is an order of magnitude lower than the barriers and their effect is negligible until frequencies are above 10 MHz. Once this impedance is known, the current flowing through the system can be calculated for any given input voltage (V_{sample}). From this a transfer function describing the relative voltage drop across the sample channel can be derived:

$$V_{sample} = I_{total} \cdot R_{sample} = \frac{V_{input}}{Z_{total}} \cdot Z_{sample}\,[\mathrm{V}] \quad (4)$$

$$\frac{V_{sample}}{V_{input}} = \frac{Z_{sample}}{Z_{total}}\left[\frac{V}{V}\right] \quad (5)$$

This transfer function lends intuition toward to the optimal frequency range for operation of these devices as it has been previously shown that cDEP devices begin to perform well when about 1% of the total voltage drop occurs across the sample channel [35]. An approximation for $|\vec{\Gamma}|$ can be achieved by finding the change in resistance (∂R) of the sample channel per unit length (∂x):

$$R_{sample}(x) = \frac{L(x)}{\sigma \cdot h \cdot w(x)}\,[\Omega] \quad (6)$$

$$\frac{\partial R}{\partial x}(x) = \frac{w(x) - x \cdot w'(x)}{\sigma \cdot h \cdot w(x)^2}\left[\frac{\Omega}{m}\right] \quad (7)$$

where h is the depth of the channel, $L(x) = x$ is the length of the sample channel segment, and $w(x)$ is the width of the channel at location x. Assuming that the current passing through vertical sections of the channel remain constant, the change in voltage per unit length can be found and a numerical approximation for $|\vec{\Gamma}|$ can be determined by:

$$\left|\vec{\Gamma}\right| \approx \left|\frac{\partial(E(x)^2)}{\partial L}\right| \approx \left|\frac{E(x_1)^2 - E(x_2)^2}{x_1 - x_2}\right|\left[\frac{V^2}{m^3}\right] \quad (8)$$

3 Methods

3.1 Numerical modeling

Two-dimensional geometries were created using AutoCAD (AutoCAD Mechanical 2010, Autodesk Inc., San Rafael, CA, USA). The geometries were imported into COMSOL Multiphysics (Version 4.2, COMSOL Inc., Burlington, MA, USA) and extruded into a 3 D geometry as shown in Fig. 1A–C. The AC/DC module was used to solve for the potential distribution, ϕ. Edges of the electrode channels were modeled as a uniform potential of 100 V or ground. The frequency of the applied signal was incrementally increased from 10^2 to 10^9 Hz using MATLAB (Version R2010b, The MathWorks Inc., Natick, MA, USA) to create a logarithmically dispersed frequency distribution. ϕ was used to calculate the magnitude of the particle-independent DEP vector ($|\vec{\Gamma}|$). This was accomplished by evaluating the partial derivatives of ϕ in the x, y, and z directions to determine the directional components of the electric field ($\vec{E}$). These values were then used to calculate $\vec{E} \cdot \vec{E}$. Finally, $|\vec{\Gamma}|$ was calculated by finding the magnitude of the partial derivatives of $|\vec{E} \cdot \vec{E}|$ in the x, y, and z directions. A representative surface plot of the $|\vec{\Gamma}|$ distribution is shown in Fig. 1D.

The numerical approximation of $|\vec{\Gamma}|$ in Eq. (8) was calculated in MATLAB based on the electrical component model shown in Fig. 1E. First, the resistance and capacitance of each element was calculated based on their geometrical properties. The total impedance of the system was then calculated and a frequency-dependent transfer function was determined. This function was multiplied by 100 V to determine the voltage drop across the sample channel at frequencies between 10^2 and 10^9 Hz. The current flowing through the channel was then calculated based on the impedance of the sample channel at each frequency.

The geometry presented here has rounded saw tooth constrictions that compress the channel from 500 to 100 μm over a distance of 400 μm. These values were used as a linear approximation of the change in channel resistance per unit channel length near the constrictions. Finally, these values were used in Eq. (8) to calculate the numerical approximation for $|\vec{\Gamma}|$.

The sample channel and fluid electrodes were prescribed conductivities of 0.01 and 1.4 S/m, respectively. Both were prescribed a relative permittivity of 80 as assumed based on their water composition. The remaining device was prescribed the material properties of either PDMS, PMMA, polyimide (PI), or PVDF. These materials were selected due to their availability in thin films and suitable electrical properties.

A parametric study was conducted to examine the effect of device geometries on the particle-independent DEP vector. Maximum and minimum values for the insulating barrier area, barrier thickness, sample channel depth, and electrode separation distance can be seen in Table 1. PDMS was used as the nominal device material except where stated otherwise.

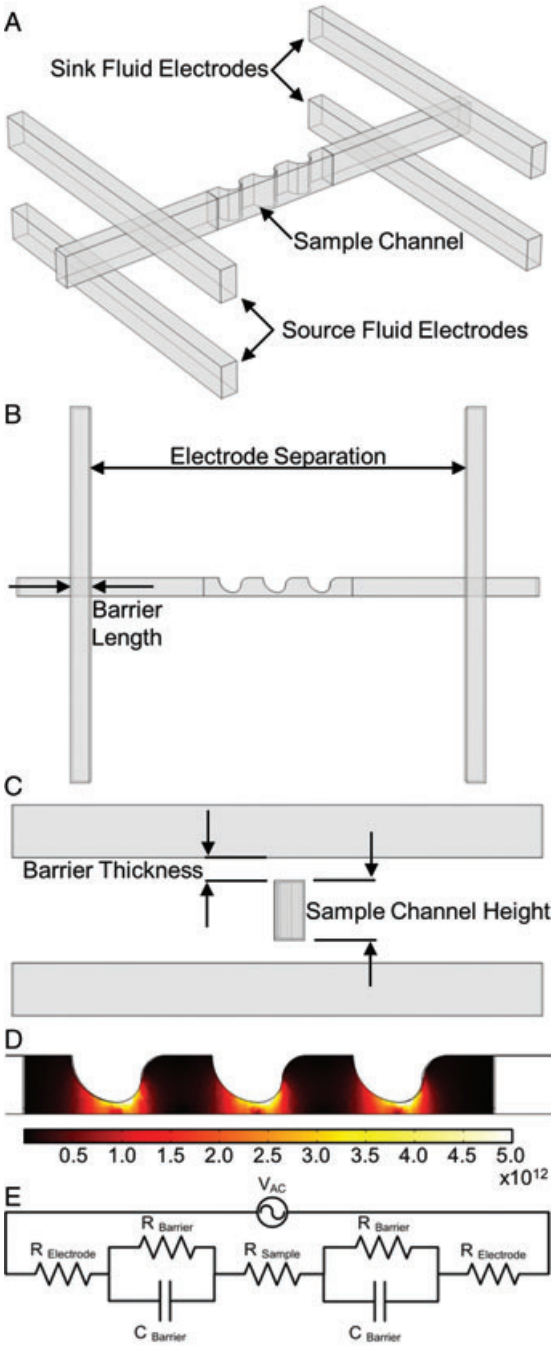

Figure 1. (A–C) Isometric, top, and side view schematics of the geometric configuration used in finite element analysis. (D) Surface plot of $|\vec{\Gamma}|$ calculated using the nominal values in Table 1 at 250 kHz. (E) Lumped element model used to calculate the numerical approximations of $|\vec{\Gamma}|$.

3.2 Cell preparation

MDA-MB-231 human breast cancer cells were cultured in DMEM/F12 media. The medium was supplemented with 10% fetal bovine serum (FBS) and 1% of penicillin/streptomycin. Cultures were maintained in solution at 37°C and 5% CO_2 in a humidified atmosphere. All cells were harvested by trypsinization at 80% confluence. The cells were suspended in a low-conductivity buffer [45], stained with CellTrace calcein red/orange (Invitrogen, Eugene, OR, USA), washed twice, and suspended again in fresh buffer to achieve a solution conductivity of 100 ± 30 μS/cm and a cell concentration of 3×10^6 cells/mL.

Table 1. Parameter values examined using finite element analysis

Parameter	Minimum	Maximum	Nominal	Unit
Barrier area	0.125	0.5	0.25	mm^2
Barrier thickness	20	100	60	μm
Sample depth	50	2000	1000	μm
Electrode separation	0.1	5	1	Cm

3.3 Experimental parameters

Devices were fabricated courtesy of Protea Biosciences (Morgantown, WV, USA). Schematic representations of the device can be seen in Fig. 1A–C. Two pairs of fluid electrode channels straddle a sample channel machined in 900-μm thick PMMA. The source and sink fluid electrode pairs were separated by 1.7 cm. One hundred twenty micrometer thick polycarbonate film layers separate the fluid electrodes from the sample channel. The nominal width of the sample channel was approximately 850 μm with "saw tooth" features along one edge that constricted the channel to approximately 600 μm. The devices were placed into a vacuum jar for at least 30 min prior to experiments to minimize bubble formation within the device during priming. The fluid electrode channels were filled with PBS (Geno Technology, St. Louis, MO, USA) and then wire electrodes were placed into the source and sink fluid electrode channels. The sample channel was primed with low-conductivity buffer (100 ± 30 μS/cm), then tubing was press fit into the inlet of the channel. The inlet tubing was connected to a 1-mL syringe containing the cell suspension via a blunt needle.

Cell suspensions were driven through the sample channel at a rate of 1.0 mL/h by a syringe pump (PHD Ultra, Harvard Apparatus, Holliston, MA, USA). An inverted light microscope (Leica DMI 6000B, Leica Microsystems, Bannockburn, IL, USA) was used to monitor the cells.

An AC electric field was created by amplifying (AL-50HF-A, Amp-Line Corp., Oakland Gardens, NY, USA) the output signal of a function generator (GFG-3015, GW Instek, Taipei, Taiwan) to a maximum of 25 V_{RMS}. A step up transformer (AL-T340.4, Amp-Line Corp.) was used to achieve output voltages up to 300 V_{RMS} at 600 kHz. Voltage and frequency were measured using an oscilloscope (TDS-1002B, Tektronics Inc. Beaverton, OR, USA) connected to the output stage of the transformer.

4 Results and discussion

4.1 Numerical modeling

A surface plot of $|\vec{\Gamma}|$ in the nominal configuration at 250 kHz is shown in Fig. 1D. The 2D slice shown is at the center of the sample channel. In COMSOL, the barrier area was sequentially increased from 0.125 to 0.5 mm^2 by increasing the width of the fluid electrode channels. Because electrode channels are filled with a highly conductive solution (PBS), their dimensions have a negligible effect on the frequency response. Increasing the barrier area effectively reduces the barrier resistance ($R = \rho d/A$) and increases the barrier capacitance ($C = \varepsilon_0 \varepsilon_r A/d$), where d is the thickness, A is the area, ρ is the resistivity, ε_r is the relative permittivity of the barrier material, and ε_0 is the permittivity of free space. This causes the impedance of the barriers to roll off at a slightly lower frequency as barrier area increases. Fig. 2A, shows that larger barrier cross-sectional areas are preferred, however, there are diminishing returns. Larger unsupported barriers may collapse into the sample channel or break. Ultimately, supportive pillars or structures may be required resulting in a tradeoff between barrier area and mechanical strength. The frequency response of the device will be negatively impacted by the addition of supportive pillars only to the extent at which they decrease the total barrier area. It is not anticipated that they will induce a strong DEP force, as the electric field is relatively constant between fluid electrodes at the same potential.

Decreasing the thickness of the barrier increases the capacitance and decreases the resistance of the barrier. The impedance of thinner barriers falls off more quickly, improving the frequency response of the device as shown in Fig. 2B. Similar mechanical considerations must be taken when decreasing the barrier thickness as when increasing the barrier cross-sectional area. In addition, the voltage at which dielectric breakdown occurs is directly dependent on the thickness of the material. PDMS for example, has a dielectric strength of approximately 20 V/μm. A device with 100 μm barriers can withstand applied voltages in excess of 2000 V_{peak}; however, a thinner barrier of 20 μm can only withstand 400 V_{peak}. These limitations must be strongly considered in device design as simulations suggest that the maximum $|\vec{\Gamma}|$ does not increase significantly as the barrier becomes thinner. If very large voltages are necessary to achieve particle manipulation, for example in the case of organelles or viral particles where the effective particle radius is very small, then thicker membranes may be required at the expense of frequency response.

Increasing the separation distance between the source and sink electrodes has a net effect of increasing the resistance of the sample channel. This in turn causes a greater proportion of the voltage drop to occur across the sample channel. The consequence of this is that for large separation distances, the $|\vec{\Gamma}|$ increases more rapidly at lower frequencies, the response reaches its maximum more quickly, and becomes "flat" over a larger frequency spectrum.

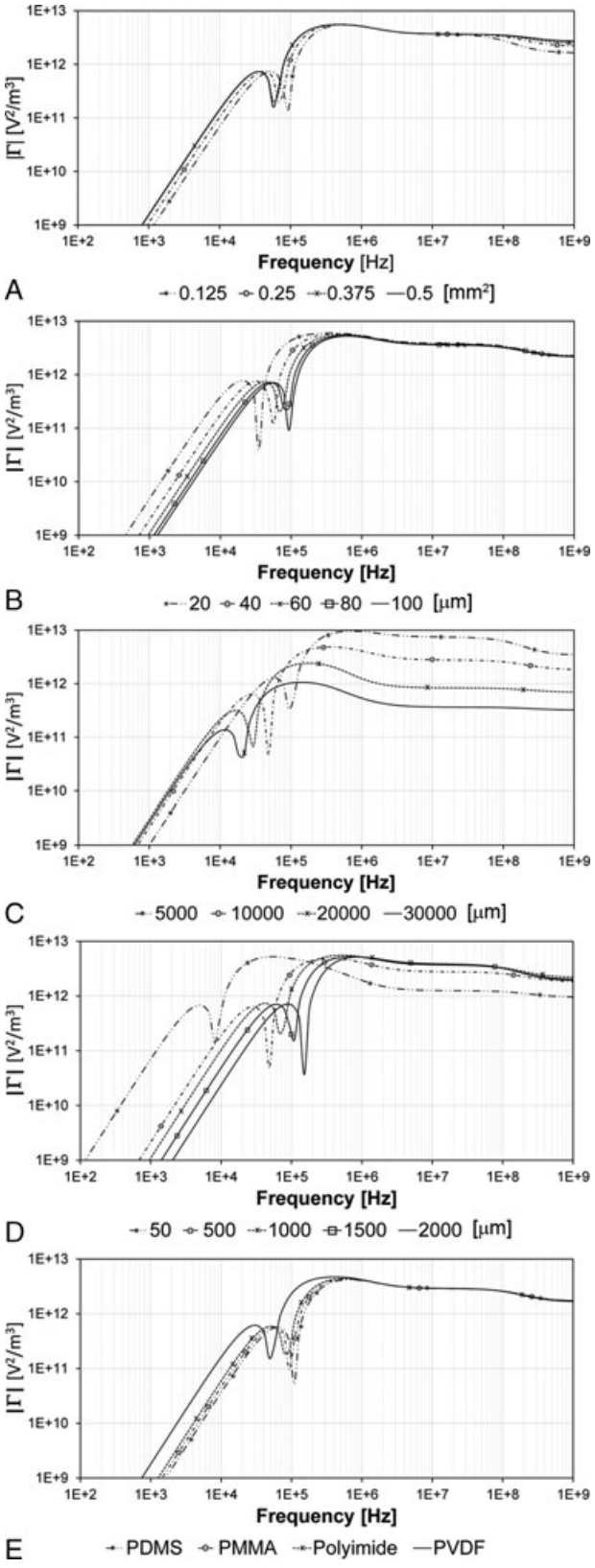

Figure 2. Finite element analysis of multilayer cDEP devices. The frequency responses of these devices change relative to (A) barrier cross sectional area, (B) barrier thickness, (C) electrode separation, (D) sample channel depth, and (E) barrier material.

For example, a $|\vec{\Gamma}| = 10^{11}$ is achieved at lower frequencies, as the electrodes are pulled apart. At the same time, as shown in Fig. 2C, the distance between the electrodes increases, causing a decrease in the change in voltage per unit length ($\partial V/\partial x$). This results in a lower maximum $|\vec{\Gamma}|$ value achieved in the sample channel. There is a tradeoff between the "flatness" of the response needed and the maximum $|\vec{\Gamma}|$ achievable for a given device.

The depth of the sample channel may have the largest impact on the performance of cDEP devices from both an operational and electrical standpoint as shown in Fig. 2D. The resistance of the sample channel increases linearly as the channel becomes shallower. This increases the total voltage drop across the sample channel, allowing for the generation of significant $|\vec{\Gamma}|$ values at lower frequencies. As the channel is made deeper, the resistance decreases and useful $|\vec{\Gamma}|$ values are pushed higher in frequency. As with barrier thickness and barrier area, the maximum achievable $|\vec{\Gamma}|$ value is independent of the depth of the sample channel. Only the frequency at which this maximum occurs is affected. As the sample channel depth increases beyond 500 μm, the effect on the frequency response becomes less significant and higher levels of throughput become accessible. For example, a multilayer device with a sample depth of 2000 μm (and all other values nominal) has similar electrical performance characteristics as some of the first cDEP devices reported [33], however, keeping bulk fluid velocities the same, the multilayer device will achieve approximately 40 times greater throughput (50-μm deep channels with a flow rate of 0.02 mL/h versus 2000-μm deep channels and flow rate of 0.8 mL/h).

The membrane used to isolate individual layers of a multilayer device does not have to be the same material as the substrate in which the microfluidic features are patterned. This allows for the investigation of materials that may have better electrical properties than traditional stamping polymers such as PDMS. There are wide range of biocompatible polymers that are readily available in thin films. Typically, these polymers have relative permittivities of approximately 3. This has to do with the similarity in density of these films and the C–M relation (K) for an assembly of $–CH_2$ polymer units:

$$\varepsilon = \frac{2K\upsilon + 1}{1 - K\upsilon} \tag{9}$$

where $K = 0.327 \times 10^{-3}$ and υ is the density of the polymer [46] .

Under the influence of a static field, the molecules of dielectric materials become polarized. In an AC field, the direction of the field oscillates. The direction of polarization of the molecules changes to follow the direction of the applied field. Because this change is not instantaneous, the polarizations of the molecules lag behind the field with a characteristic time known as the relaxation time. This time is typically on the order of 10^{-11} s. For the frequencies studied here, the relaxation time for the barrier materials are considered negligible and the relative permittivity is held constant at all frequencies.

Table 2. Electrical properties of membrane materials

Material	Relative permittivity	Resistivity [Ω-cm]	Dielectric strength [V/μm]
PDMS	2.65	1.2×10^{14}	20.0
PMMA	3.3	1.0×10^{15}	20.0
PI	3.5	1.0×10^{12}	12.0
PVDF	9	1.0×10^{14}	10.0

For membranes made of PDMS, PI, and PMMA, there is no significant change in the frequency response of the devices when all of these materials are of the same thickness, as shown in Fig. 2E. The electrical properties of these materials, derived from manufacturers data sheets, are presented in Table 2. The relative permittivity of PVDF, approximately 9.0, gives the material a higher capacitance per unit thickness. Devices using this material as the insulating barrier between layers reach their maximum $|\vec{\Gamma}|$ at lower frequencies. This increases the frequency range over which the devices exhibit a flat DEP response. The maximum $|\vec{\Gamma}|$ is nearly equivalent between each of these materials. This is advantageous as it allows for barrier materials selection to be made based on manufacturing and mechanical considerations.

PDMS films of predictable thickness can readily be fabricated by spin coating the polymer on a flat surface and procedures for PDMS–PDMS bonding are well documented in the literature [47]. Commercially available films are generally available in thicknesses of 25.3 μm (0.001 inches), however some specialty films, such as polyimide are available in thicknesses of 7.5 μm or less under brand names of Kapton and Corin XLS. These materials are advantageous over thicker films as they will have a lower net resistance and increased capacitance improving device performance, however, their breakdown voltages will be drastically reduced. In the case of a 7.5-μm polyimide film, operating voltages would be limited to those less than 90 V_{peak}. It should be noted that AC voltages are often applied and measured in terms of the root mean square (RMS) of the peak-to-peak voltage. The corresponding AC breakdown voltage of a 7.5-μm polyimide film will be $\sqrt{2}$ times less than the DC voltage, or 64.6 V_{RMS}.

Eq. (8) was used to conduct an additional parametric analysis for comparison with the results determined in COMSOL. This model used nominal values of 2×10^6 [Ω], 2.86×10^4 [Ω], 2.89×10^{14} [Ω], and 9.77×10^{-14} [F] for the sample resistance, fluid electrode resistance, barrier resistance, and barrier capacitance in Eq. (3). These values represent the approximate values of the nominal multilayer device used in the multiphysics simulations. The effect of increasing barrier capacitance is shown in Fig. 3A. A tenfold increase in barrier capacitance resulted in a frequency response that reaches the maximum $|\vec{\Gamma}|$ value, an order of magnitude before the nominal case. This trend matches the results determined via finite element modeling of decreasing barrier thickness and increasing barrier cross-sectional area and help to validate the use of strictly numerical solutions to analyze cDEP devices.

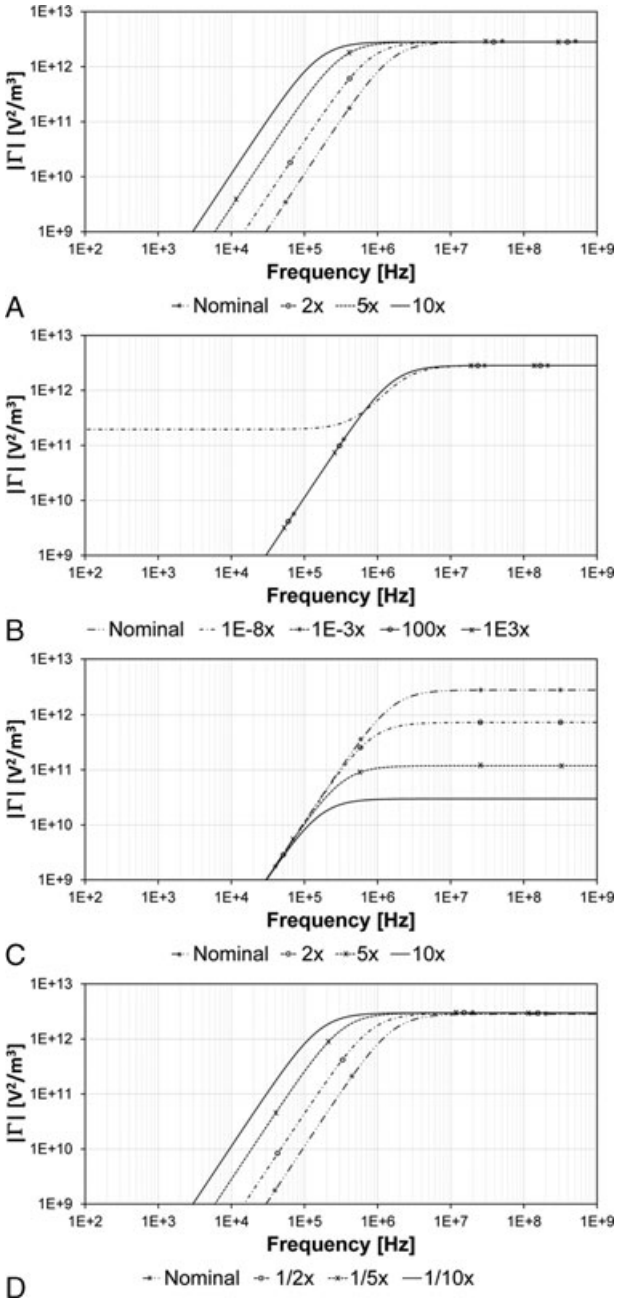

Figure 3. Numerical approximation of $|\vec{\Gamma}|$ in multilayer cDEP devices. The frequency responses of these devices change relative to (A) barrier capacitance, (B) barrier resistance, (C) electrode separation, (D) and sample channel depth.

The resistance of the barrier plays a minimal role in the performance of these devices as shown in Fig. 3B. It is not until the resistance of the barrier (or resistivity of the material) is decreased eight orders of magnitude that this component makes a significant contribution. In that case, the resistances of the barrier and of the sample channel are of similar order of magnitude. This minimal effect of barrier resistance is due to the capacitive elements of the barriers that cause their impedance to start rolling off at very low frequencies.

Increasing only the resistance of the sample channel in Eq. (3), similar to pulling the fluid electrodes further apart, decreases the maximum $|\vec{\Gamma}|$ value achieved. This trend, shown in Fig. 3C, is due to the model representing the total voltage dropping over a longer distance, so the change in voltage per unit length becomes smaller. A tenfold increase in sample channel resistance resulted in a two order of magnitude drop in the maximum $|\vec{\Gamma}|$ value. However, the higher resistance sample channels have linear frequency responses over a larger frequency range.

This method was also used to model the effect of reducing the sample channel depth. Here, the resistance of the sample channel was increased in Eq. (3) and the height of the sample channel was changed proportionately in Eq. (7). A tenfold decrease in sample height resulted in a $|\vec{\Gamma}|$ that reached its maximum at frequency an order of magnitude lower. These results, shown in Fig. 3D, also exhibit the same trend found in the multiphysics simulations shown in Fig. 2D.

These results show that approximating $|\vec{\Gamma}|$ numerically yield similar results and trends as compared to the more computationally demanding finite element methods. While this method cannot predict the spatial distribution of the electric field, it can be used to generate order of magnitude approximations and explore the implications of specific changes in device geometry.

The numerical approximation of $|\vec{\Gamma}|$ (Fig. 3) predicts a smooth increase and plateau anticipated for a simple resistor–capacitor circuit. The finite element solutions (Fig. 2) exhibit a sharp drop in $|\vec{\Gamma}|$ just prior to it reaching its maximum. This indicates the presence of losses, resonance, or inductance that are not accounted for in the numerical approximation. This behavior was not evident in our previous experimental work, though it may have been confounded by changes in the C–M factor, for the cells evaluated, at these transient frequencies.

4.2 Experimental results

A top down view of the multilayer prototype device is shown in Fig. 4A. In the absence of an electric field, cells flowed freely through the device as shown in Fig. 4B. When a 250 V_{RMS} potential at 600 kHz was applied, individual cells were observed migrating towards each other forming "pearl chains." This initial indication of the presence of a strong electric field continued at time progressed and successively longer chains of cells formed within the device. These chains, and individual cells, began to migrate toward the "saw tooth" features along the bottom edge of the sample channel and become immobilized. After approximately 1 min, a large number of cells had become trapped as shown in Fig. 4C. Long chains of cells continued to slide along the bottom edge of the device, just above the trapped cells.

This is the first demonstration of DEP in a device in which fluid electrodes are fabricated in separate substrates

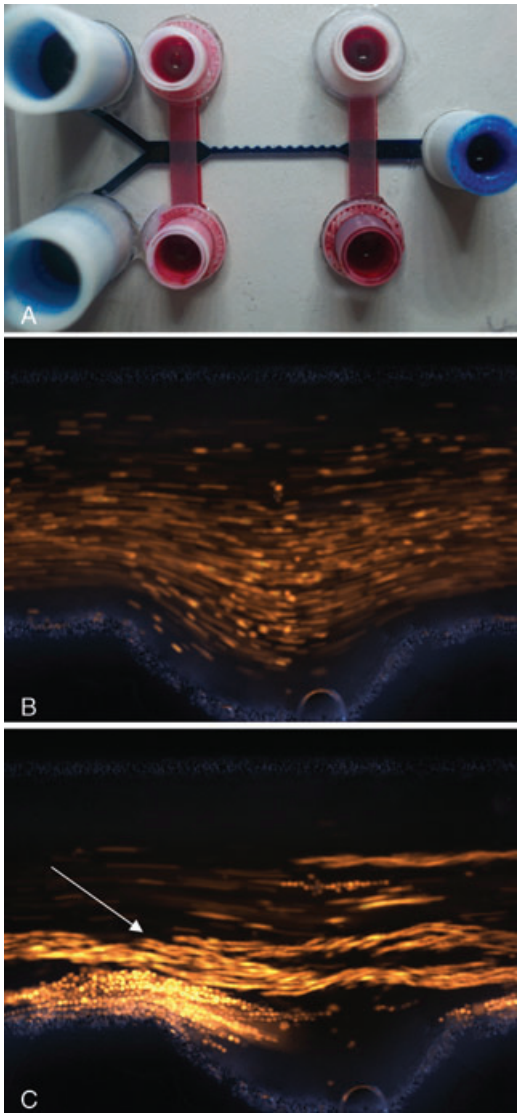

Figure 4. (A) A prototype multilayer cDEP device with fluid electrode channels (red) above and below the sample channel (blue). (B) Cells pass freely through the device when the electric field is turned off. (C) Under the influence of a 250 V_{RMS} electric field oscillating at 600 kHz, cells form "pearl chains," indicated by the white arrow, and become immobilized near the saw tooth features at the edge of the sample channel.

and physically isolated from the sample channel by a thin film. These preliminary results show that it is possible to generate an electric field within the sample channel of a multilayer cDEP device. The dielectrophoretic force generated was great enough to trap cells being driven at a flow rate of 1.0 mL/h. This represents a 100-fold increase in flow rate compared to this geometry fabricated in a single layer of PDMS [35]. Future work will focus on producing devices with thinner membranes between the sample and fluid electrode layers, measuring the electrical characteristics of the devices, and evaluating the response of cells across a wide frequency spectrum.

5 Concluding remarks

Here, we presented the geometrical considerations necessary to produce a multilayer cDEP device that achieves a high level of throughput while maintaining sufficient electric field nonuniformity to manipulate cells. These devices in their nature have a frequency response that must be understood when interpreting experimental results. For this reason, the C–M factor was decoupled from the ability of the device to produce highly nonuniform electric fields. From an experimental standpoint, production of high-voltage, high-frequency electrical signals becomes challenging above 1 MHz. Below 1 MHz, ionic and dipole relaxation are expected to influence cells with the former dominating over the later at lower frequencies. Ultimately, the electrical and physical properties of the cytoplasm, cellular, and nuclear membranes will affect the dielectrophoretic response.

This work is the first description of a multilayer cDEP device. Analysis was completed using both finite element software and a more efficient numerical approximation. The nonuniform electric field generated within these multilayer devices is comparable to the single-layer devices presented previously [37]. While the numerical approximation does not capture some of the intricate fluctuations in the frequency response, it provides an order of magnitude approximation. This approximation is significantly less computationally demanding than the 3D finite element solution taking seconds rather than hours to compute frequency responses for each parameter. This numerical approximation can be adapted for calculation using open source spreadsheet software, providing a less computationally demanding means to model complex cDEP devices. Additionally, this method should provide a reasonable approximation for other insulator-based DEP devices.

We demonstrated trapping of MDA-MB-231 breast cancer cells in a prototype device at a flow rate of 1.0 mL/h. This represents a significant increase in throughput over previously reported cDEP devices. Future work will focus refining fabrication of these devices and demonstrating their ability to sort heterogeneous cell populations.

Of the parameters affecting device performance, electrode separation distance had the largest influence on the frequency response. This parameter was also the only one that significantly influenced the maximum value of $|\vec{\Gamma}|$. This has to do with losses associated with regions of the sample channel between the electrodes not containing constricting features. Consequently, if higher $|\vec{\Gamma}|$ values are needed in conjunction with a low-frequency response, a higher input voltage must be applied. The ultimate limiting factors in device performance then reside in breakdown voltage of the barrier material and the ability to generate high-frequency signals at high voltages.

This work was supported in part by the Institute for Critical Technology and Applied Science (ICTAS) at Virginia Tech. The authors would like to thank the members of the BEMS laboratory for their help with editing this document and Trust Razunguzwa,

Matthew Powell, and Jordan Friend for their assistance in fabricating the prototype devices.

The authors have declared the following potential conflict of interest: Sano and Davalos have a pending patent in Contactless Dielectrophoresis.

6 References

[1] Pohl, H. A., *J. Appl. Phys.* 1951, *22*, 869–871.

[2] Pohl, H. A., Schwar, J. P., *J. Electrochem. Soc.* 1960, *107*, 383–385.

[3] Pohl, H. A., Hawk, I., *Science* 1966, *152*, 647-a-649.

[4] Fuhr, G., Hagedorn, R., Muller, T., Wagner, B., Benecke, W., *Micro Electro Mechanical Systems, 1991, MEMS '91, Proceedings. An Investigation of Micro Structures, Sensors, Actuators, Machines and Robots*, IEEE, San Diego, CA 1991, pp. 259–264.

[5] Cui, L., Holmes, D., Morgan, H., *Electrophoresis* 2001, *22*, 3893–3901.

[6] Choi, E., Kim, B., Park, J., *J. Michromech. Microeng.* 2009, *19*, 125014.

[7] Goater, A. D., Burt, J. P. H., Pethig, R., *J. Phys. D Appl. Phys.* 1997, *30*, L65–L69.

[8] Talary, M. S., Burt, J. P. H., Tame, J. A., Pethig, R., *J. Phys. D Appl. Phys.* 1996, *29*, 2198–2203.

[9] Docoslis, A., Kalogerakis, N., Behie, L. A., Kaler, K., *Biotechnol. Bioeng.* 1997, *54*, 239–250.

[10] Asbury, C. L., van den Engh, G., *Biophys. J.* 1998, *74*, 1024–1030.

[11] Muller, T., Fiedler, S., Schnelle, T., Ludwig, K., Jung, H., Fuhr, G., *Biotechnol. Tech.* 1996, *10*, 221–226.

[12] Archer, S., Li, T. T., Evans, A. T., Britland, S. T., Morgan, H., *Biochem. Biophys. Res. Commun.* 1999, *257*, 687–698.

[13] Srivastava, S. K., Daggolu, P. R., Burgess, S. C., Minerick, A. R., *Electrophoresis* 2008, *29*, 5033–5046.

[14] Hwang, H., Lee, D. H., Choi, W. J., Park, J. K., *Biomicrofluidics* 2009, *3*, 014103.

[15] Leonard, K. M., Minerick, A. R., *Electrophoresis* 2011, *32*, 2512–2522.

[16] Martinez-Duarte, R., Renaud, P., Madou, M. J., *Electrophoresis* 2011, *32*, 2385–2392.

[17] Wang, L., Flanagan, L. A., Jeon, N. L., Monuki, E., Lee, A. P., *Lab Chip* 2007, *7*, 1114–1120.

[18] Lewpiriyawong, N., Kandaswamy, K., Yang, C., Ivanov, V., Stocker, R., *Anal. Chem.* 2011, *83*, 9579–9585.

[19] Cummings, E. B., Singh, A. K., *Anal. Chem.* 2003, *75*, 4724–4731.

[20] Lapizco-Encinas, B. H., Ozuna-Chacon, S., Rito-Palomares, M., *J. Chromatogr. A* 2008, *1206*, 45–51.

[21] Baylon-Cardiel, J. L., Jesus-Perez, N. M., Chavez-Santoscoy, A. V., Lapizco-Encinas, B. H., *Lab Chip* 2010, *10*, 3235–3242.

[22] Davalos, R. V., Lapizco-Encinas, B. H., Fiechtner, G. J., Singh, A. K., Simmons, B. A., Fintschenko, Y., Cummings, E. B., *Roy. Soc. Chem.* 2004, *1*, 650–652.

[23] Lapizco-Encinas, B. H., Simmons, B. A., Cummings, E. B., Fintschenko, Y., *Electrophoresis* 2004, *25*, 1695–1704.

[24] Davalos, R. V., McGraw, G. J., Wallow, T. I., Morales, A. M., Krafcik, K. L., Fintschenko, Y., Cummings, E. B., Simmons, B. A., *Anal. Bioanal. Chem.* 2008, *390*, 847–855.

[25] Mela, P., van den Berg, A., Fintschenko, Y., Cummings, E. B., Simmons, B. A., Kirby, B. J., *Electrophoresis* 2005, *26*, 1792–1799.

[26] Moncada-Hernandez, H., Baylon-Cardiel, J. L., Pérez-González, V. H., Lapizco-Encinas, B. H., *Electrophoresis* 2011, *32*, 2502–2511.

[27] Weiss, N. G., Jones, P. V., Mahanti, P., Chen, K. P., Taylor, T. J., Hayes, M. A., *Electrophoresis* 2011, *32*, 2292–2297.

[28] Bhattacharya, S., Chao, T.-C., Ros, A., *Electrophoresis* 2011, *32*, 2550–2558.

[29] Ivory, C. F., Srivastava, S. K., *Electrophoresis* 2011, *32*, 2323–2330.

[30] Gallo-Villanueva, R. C., Rodriguez-Lopez, C. E., Diaz-De-La-Garza, R. I., Reyes-Betanzo, C., Lapizco-Encinas, B. H., *Electrophoresis* 2009, *30*, 4195–4205.

[31] Gallo-Villanueva, R. C., Pérez-González, V. H., Davalos, R. V., Lapizco-Encinas, B. H., *Electrophoresis* 2011, *32*, 2456–2465.

[32] Srivastava, S. K., Artemiou, A., Minerick, A. R., *Electrophoresis* 2011, *32*, 2530–2540.

[33] Shafiee, H., Caldwell, J. L., Sano, M. B., Davalos, R. V., *Biomed. Microdevices* 2009, *11*, 997–1006.

[34] Park, K., Suk, H.-J., Akin, D., Bashir, R., *Lab Chip* 2009, *9*, 2224–2229.

[35] Sano, M. B., Caldwell, J. L., Davalos, R. V., *Biosens. Bioelectron.* 2011, *30*, 13–20.

[36] Pethig, R., Markx, G. H., *Trends Biotechnol.* 1997, *15*, 426–432.

[37] Shafiee, H., Sano, M. B., Henslee, E. A., Caldwell, J. L., Davalos, R. V., *Lab Chip* 2010, *10*, 438–445.

[38] Shafiee, H., Caldwell, J. L., Davalos, R. V., *JALA* 2010, *15*, 224–232.

[39] Salmanzadeh, A., Romero, L., Shafiee, H., Gallo-Villanueva, R., Stremler, M., Cramer, S., Davalos, R., *Lab Chip* 2011, *12*, 182–189.

[40] Henslee, E. A., Sano, M. B., Rojas, A. D., Schmelz, E. M., Davalos, R. V., *Electrophoresis* 2011, *32*, 2523–2529.

[41] Sano, M. B., Henslee, E. A., Schmelz, E., Davalos, R. V., *Electrophoresis* 2011, *32*, 3164–3171.

[42] Pohl, H. A., Plymale, C. E., *J. Electrochem. Soc.* 1960, *107*, 390–396.

[43] Henslee, E. A., Sano, M. B., Rojas, A. D., Davalos, R. V., *Electrophoresis* 2011, *32, 2523–2529.*

[44] Gagnon, Z. R., *Electrophoresis* 2011, *32*, 2466–2487.

[45] Flanagan, L. A., Lu, J., Wang, L., Marchenko, S. A., Jeon, N. L., Lee, A. P., Monuki, E. S., *Stem Cells* 2008, *26*, 656–665.

[46] Blythe, A. R., Bloor, D., *Electrical Properties of Polymers*, Cambridge University Press, Cambridge, NY 2005.

[47] Eddings, M. A., Johnson, M. A., Gale, B. K., *J. Michromech. Microeng.* 2008, *18*, 067001.

